Desalination and Water Treatment
www.deswater.com

doi: 10.5004/dwt.2022.29031

280 (2022) 206–223
December

Green magnetic clay nanocomposite based on graphene oxide nanosheet as a synthetic low-cost adsorbent for oil droplets removal from produced water

Alshimaa M. Ahmed[a,*], R. Hosny[b,*], Mahmoud F. Mubarak[c,*], Ahmed A. Younes[a], A.B. Farag[a]

[a]*Chemistry Department, Faculty of Science, Helwan University, Cairo, Egypt, email: alshimaamaher2014@yahoo.com (A.M. Ahmed)*
[b]*Production Department, Egyptian Petroleum Research Institute (EPRI), 1 Ahmed El-Zomor, P.O. 11727, Nasr City, Cairo, Egypt, Tel.: +(202)22747847; Fax: +(202)22747433; email: rashahosny@epri.sci.eg/dr.rashahosny@yahoo.com (R. Hosny)*
[c]*Petroleum Application Department, Egyptian Petroleum Research Institute (EPRI), 1 Ahmed El-Zomor, P.O. 11727, Nasr City, Cairo, Egypt, Tel.: +(202)22747847; Fax: +(202)22747433; email: fathy8753@yahoo.com (M.F. Mubarak)*

Received 23 June 2022; Accepted 4 October 2022

ABSTRACT

A green magnetic nanocomposite based on kaolin clay and two-dimension graphene oxide (Fe_3O_4@GO@Ka) was prepared using natural, economic, and available raw materials for oil removal from produced water. The preparation was carried out through a two-step hydrothermal carbonization method followed by a modified co-precipitation method in the presence of a kaolin clay matrix. Fourier-transform infrared spectroscopy, X-ray diffraction, scanning electron microscopy, high-resolution transmission electron microscopy, Brunauer–Emmett–Teller, and vibrating-sample magnetometer, were used to characterize Fe_3O_4@GO@Ka. The batch experiments results revealed that the oil removal efficiency reached its maximum with contact time = 60.0 min, pH = 7.0, initial oil concentration = 25.0 mg/L, the composite quantity = 5.0 mg, and T = 35°C. Theoretical models were applied to examine and assess the adsorption kinetics and isotherm. The adsorption kinetic was found to follow the pseudo-second-order, implying that the emulsified oil adsorption mechanism is chemisorption. The isothermal results closely matched the Freundlich isotherm model, meaning that the adsorption occurs in multilayers on a heterogeneous surface. Thermodynamic studies indicated that the adsorption process was spontaneous and endothermic. The prepared nanocomposite was regenerated using ethanol and reused four times without a significant decrease in its oil removal efficiency. These results indicated that Fe_3O_4@GO@Ka could be a promising, eco-friendly adsorbent for removing emulsified oil droplets.

Keywords: Nanocomposite; Produced water; Magnetite; Graphene oxide; Kaolin; Hydrothermal carbonization

1. Introduction

During crude oil and gas extraction, vast amounts of wastewater are generated. This wastewater is called produced water (PW), this water is polluted with petroleum, and other pollutants (including solids, toxic organic matters, metals, and the chemicals employed in the manufacturing process), contaminating the ecosystem if not correctly disposed of [1–6]. Oil and grease in PW can appear in free, dispersed, emulsified, or dissolved forms [7,8]. Because of their toxicological and aesthetic effects, emulsified oil droplets found in these generated waters are a source of worry [5,9,10]. Furthermore, these little droplets are more challenging to remove than free or dispersed oil, containing more significant droplet sizes because of the stable oil film generated by surfactants [10,11]. Suppose these tiny oil droplets are not removed from the water and dumped into the environment; in that case, they can

* Corresponding authors.

be dangerous to the aquatic ecology and cause high levels of biochemical oxygen demand (BOD) [9,12,13]. Due to the large amount and harmful nature of this water, it is vital to develop cost-effective and portable technology to remove emulsified oil. When PW treatment is done correctly, vast amounts of treated water can be reused and recycled, and oil can be recovered, increasing the economic and environmental sustainability of the process [5,10].

Various chemical, physical and biological technologies, including skimming, gravity setting [13,14], filtration, flotation [13–15], membrane techniques [15–18], flocculation [4], flotation [14,15,17,19], chemical coagulation [13,19], chemical oxidation [19], and electrochemical oxidation [17,19] have been developed and studied to remove emulsified oil droplets from PW. However, because most of these approaches are costly, time-consuming, secondary pollutants formation, membrane fouling [20], and low removal efficiency, and considerable research efforts have been focused on more efficient oil clean-up procedures, such as adsorption [1,5,13,21,22]. Because of its harmless and straightforward operation, suitable discharge amount, low operational cost, minimum biological sludge generation, requiring fewer chemicals, and high oil removal efficiency, the adsorption technique has shown to be one of the most effective strategies for eliminating emulsified oil [1,21,23].

Activated carbon, biopolymers, organoclay, sawdust, vermiculite, walnut shells, and resins have been investigated as adsorbents for de-oiling from oil-in-water emulsions [2,13]. In this perspective, low-cost, plentiful, safe, and renewable materials should be prioritized [24].

Kaolin is one of the distinguished natural clay substances with (1:1) layered structure that has demonstrated promising potential as an adsorbent for wastewater purification due to its low cost, nontoxicity, accessibility, large specific surface area, good chemical stability, physical, mechanical, and structural properties [25–30]. Kaolin has been commonly employed as a sustainable biosorbent for organic materials removal [24,31,32]. Some recent studies on kaolin as a membrane for oil/water emulsion separation have recently been conducted, with promising results [33,34]. More crucially, modifying clay minerals like kaolin can increase the number of adsorption sites and functional groups on their surfaces, considerably enhancing the clay minerals' adsorption ability for environmental contaminants [27,35]. Based on that, various clay mineral modification technologies have been developed in recent years [27,28,35–37]. Carbon-based nanomaterials, such as graphene-based materials, have wide applications as adsorbents for water purification due to their considerable specific surface area, excellent mechanical properties, and layered structure [10,38,39]. Graphene oxide (GO) is one of the most intensively studied graphene-based substances that is the oxidized version of graphene [40,41]. GO was added to the solution as an additive to improve the removal efficiency [28,37]. It has a variety of oxygen-containing active functional groups on its surface, such as carboxyl, carbonyl, epoxide, and hydroxyl, making it a good choice for target-specific adsorption [37,40–42]. These active oxygen functional groups give GO hydrophilic properties and make the surface modifications of GO easier, leading to the creation of other graphene-based materials [40,41]. These groups give GO surface a negative charge and enable it to interact with positively charged ions like heavy metals [43], dyes [44,45], and other organic molecules [45,46]. The GO basal plane can also interact with the aromatic rings of many organics via Π–Π interaction, as observed in previous studies [46–48]. Also, GO has been investigated as emulsified oil sorbents [10,49].

Magnetic modification has attracted much attention due to overcoming challenging separation and recovery of spent adsorbent from the solution, enhancing the adsorption property [23,26,30]. Various studies have shown that iron-based nanocomposites improve the removal efficiency of organic pollutants [26,47], heavy metals [28,50], and emulsified oil [51] from wastewater.

Herein, a green, eco-friendly synthesis route for preparing the magnetic graphene oxide/kaolin (Fe_3O_4@GO@Ka) nanocomposite was done by the hydrothermal carbonization method using affordable, natural resources (i.e., naturally occurring aluminosilicates, and glucose, a cheap, green chemical) to remove emulsified oil droplets from produced water. Fourier-transform infrared spectroscopy (FT-IR), X-ray diffraction (XRD), scanning electron microscopy (SEM), high-resolution transmission electron microscopy (HR-TEM), Brunauer–Emmett–Teller (BET) and vibrating-sample magnetometer (VSM) were used to characterize the synthesized Fe_3O_4@GO@Ka nanocomposite. The impacts of several parameters, including contact time, pH of emulsion, initial oil droplets concentration, composite quantity, and temperature, on the oil droplets adsorption process, were examined, and the optimal adsorption conditions were addressed. Furthermore, the collected data during the batch experiments were used to investigate the adsorption kinetics, isotherm, and thermodynamic behavior of the current adsorption process. Moreover, a study on the reusability of the prepared Fe_3O_4@GO@Ka nanocomposite was also carried out.

2. Experimental setup

2.1. Materials

Kaolin clay ($Al_2Si_2O_5(OH)_4$) was obtained from Sigma-Aldrich (Egypt) and was purified before use. D(+) glucose monohydrate ($C_6H_{12}O_6{\cdot}H_2O$), which is used as a precursor and ammonia solution (NH_4OH, 25%) were purchased from Pioneer for Chemical Co., (Giza, Egypt). Ferrous chloride tetrahydrate ($FeCl_2{\cdot}4H_2O$), ferric chloride hexahydrate ($FeCl_3{\cdot}6H_2O$), magnesium oxide (MgO_2) were used as a catalyst. Phosphoric acid (H_3PO_4, 85%), hydrochloric acid (HCl 36%), and sodium hydroxide (NaOH) were obtained from El-Nasr Pharmaceutical Chemicals Co., (ADWIC). Crude oil was obtained from an Egyptian oil field. Sodium dodecyl sulfate (SDS, $C_{12}H_{25}OSO_3Na$) was obtained from Techno Pharmchem Co., (New Delhi, India) and used for preparing oil in water emulsion. Ethanol (C_2H_6O 96%) was purchased from Brand Chemicals Co., (Egypt). Throughout all experiments, distilled water was used for preparing solutions.

2.2. Beneficiation and activation of kaolin

Powder kaolin was treated to remove soluble impurities and intermediate to coarse associated mineral particles

through the dispersion and decantation method [52–55] with some alteration. 40 g of kaolin was soaked in a 500 mL glass beaker containing 400 mL distilled water for 30 min with stirring, then let to settle for 3 d until the clay and water were separated into two layers by the effect of gravity. The top layer (water) was removed and distilled water was added to the solid layer (clay slurry) for the clay to be purified even more (repeated five times). The bulk clay was then dried in an oven at 109°C for 8 h. The dry clay was ground into a fine powder using a mortar pestle and sieved through a 125 μm sieve. For activation, the sieved clay was put in a crucible and thermally calcined at 500°C for 2 h in a muffle furnace to convert it to activated kaolin in metaphase [52,56].

2.3. Synthesis of hydrochar/kaolin nanocomposite (HC@Ka)

Firstly, hydrochar/kaolin nanocomposite (HC@Ka) was prepared by hydrothermal carbonization method with assist of H_3PO_4, reported by [57–59] with some alteration. In brief, 12.5 g of glucose was dissolved in 25 mL distilled water for 30 min by stirring with a magnet. Then, 2.0 g of activated kaolin clay was added to the glucose solution (2.5 M) with continuous stirring for 10 min; after that, the mixture was transferred with 7.5 mL H_3PO_4 in an impregnation ratio of (0.5:1) (H_3PO_4:glucose) into 100 mL Teflon-lined stainless steel autoclave kept at 180°C for 4 h. The autoclave was then allowed to cool to ambient temperature. The obtained solid product was filtered and washed with 10 mL NaOH (1 M) then with distilled water several times until the filtrate became colorless. Finally, the hydrochar/kaolin nanocomposites was dried at 70°C overnight in a vacuum oven.

2.4. GO@Ka nanocomposite preparation

GO@Ka nanocomposite was obtained through thermal carbonization of hydrothermally prepared hydrochar/kaolin nanocomposites (HC@Ka) [60], with the assistance of a catalyst (MgO_2) [61–64]. Briefly, the carbonaceous solid product was mixed with magnesium oxide by the ratio of 0.1% of solid product and calcination at 800°C for 2 h under a nitrogen atmosphere to obtain graphene oxide nanosheet. The obtained graphitized material was washed with distilled water many times to remove the catalyst from the graphitized material and was dried at room temperature for 2 d.

2.5. Synthesis of Fe_3O_4@GO@Ka nanocomposite

As indicated in prior work, the co-precipitation procedure was used to prepare the Fe_3O_4@GO@Ka nanocomposite [50,65–67]. $FeCl_3{\cdot}6H_2O$ and $FeCl_2{\cdot}4H_2O$ solutions were dissolved in 200 mL of distilled water with a molar ratio of 2:1 (0.0037 M and 0.0025 M) and combined with 3 g (GO@Ka) nanocomposite under vigorous mechanical stirring at 80°C, where the ratio of magnetite:(GO@Ka) was 1:10. Afterwards, 70 mL of 25% NH_4OH solution was added to precipitate magnetite at pH 10.5. The prepared composite was filtered and rinsed many times with distilled water until pH reached 6.7; after that, it was dried for 2 d at room temperature (Fig. 1).

2.6. Adsorbent characterization

The functional groups of kaolin, GO@Ka, and Fe_3O_4@GO@Ka were determined using an (FT-IR Model Spectrum One, PerkinElmer, USA). In the range of 4,000–400 cm^{-1}, the spectra were acquired using KBr pellets with a resolution of 16 cm^{-1}. X-ray diffractometer (XRD, Shimadzu XD-l) operating at 40 kV and 40 mA was used to record the X-ray diffraction (XRD) pattern of samples between 2θ of 4°–80° at a scan rate of 4°/min with a Cu-Ka radiation (λ = 0.154 nm), and a sampling angle interval of 0.02°. Transmission electron microscopy (TEM) with an acceleration voltage of 200 kV (HR-TEM, Model JEOL, JEM2100FS, Japan) and scanning electron microscopy (SEM, ZEISS-EVO 10) were used to investigate the size of particles and surface morphology of the samples. The surface area, pore volume, and pore diameter of specimens were determined using a (BET, model BELSORP, BEL Master – Ver 7.1.0.0, MicrotracBEL, Corp)

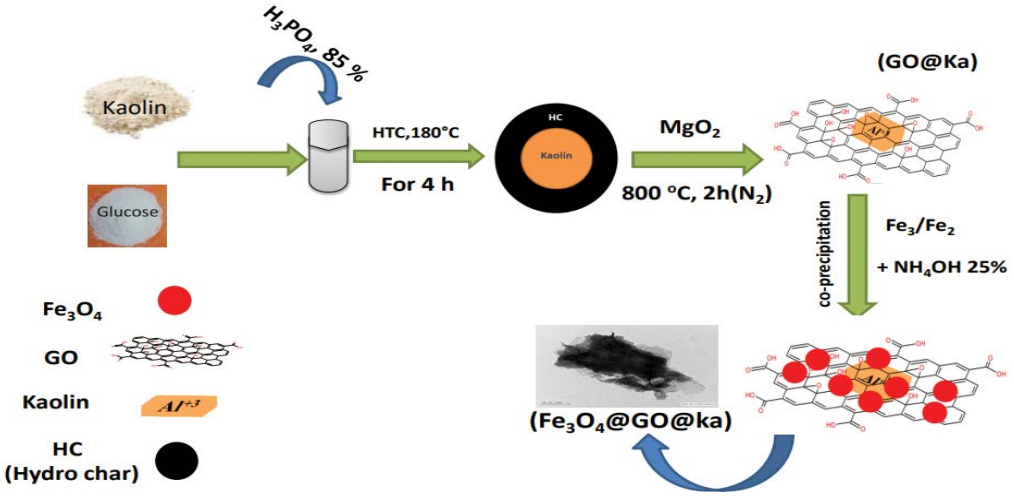

Fig. 1. Scheme of the Fe_3O_4@GO@Ka nanocomposite preparation.

through Brunauer–Emmett–Teller (BET) method, and nitrogen was used as adsorbent at 77 K. A vibrating-sample magnetometer (VSM), (Lakeshore 665; Lake Shore Cryotronics, Inc., Westerville, OH, USA) was used to measure the magnetization of Fe_3O_4 NPs and Fe_3O_4@GO@Ka nanocomposite at 308 K.

2.7. Oil-in-water emulsion preparation

The synthetic oil/water emulsion solution was made based on [68–70] with some alteration by dissolving 10 μg anionic surfactant (sodium dodecyl sulfate) in 1 L deionized water with stirring at 3,500 rpm on a magnetic stirrer for 5 min. According to the results of the stability test, this amount of surfactant is the right amount to produce a homogeneous oil/water emulsion. Since, SDS surfactant molecules operate as an adsorbent at the oil/water interface in oil/water emulsion systems, forming a negatively charged protective interfacial coating that prevents the coalescence of the emulsified oil droplets. Therefore, the low SDS concentration lead to decrease stability of oil/water emulsions and lead to coalescence of the emulsified oil droplets easily with time. Then 0.3 g crude oil was added and blended for 10–15 min with water to generate a homogeneous oil/water emulsion with a 300 mg/L oil droplets concentration. After that, the stock solution was diluted to various concentrations (250, 150, 50, and 25 mg/L). The oil/water emulsions utilized in this study were prepared fresh and used immediately.

2.8. Batch adsorption experiment

Batch adsorption experiments were performed by adding a 25 mL of oil/water emulsion (pH 7.0) to 5 mg adsorbent in a 50 mL conical flask at 35°C using a 350 rpm shaker water bath. The effects of contact time, pH of emulsion, initial concentration of emulsified oil, composite quantity, and temperature on the adsorption capacity and the removal efficiency of the Fe_3O_4@GO@Ka nanocomposite for emulsified oil droplets were investigated. The contact time effect was investigated throughout a time range of (0–60 min), with initial oil droplets concentration (C_o = 25.0 mg/L), pH (7.0), and adsorbent dose (5 mg) at 35°C. All batch studies occurred for 60min, except for the kinetic trials. The influence of solution pH was studied at a pH between 2 to 11. Here, HCl solution (0.1 M) and NaOH solution (0.1 M) were used to change the values of the pH of the emulsion. Initial emulsified oil concentrations (25–250 mg/L) were employed to evaluate the concentration effect. The impact of composite quantity was examined using various amounts of adsorbent in a range of 1–9 mg. The adsorption thermodynamics studies were investigated at different temperature values (25°C, 30°C, 35°C, 50°C, and 60°C). Kinetic studies were carried out over various times, with a Fe_3O_4@GO@Ka dose (5 mg) and an initial emulsified oil concentration of (C_o = 25.0 mg/L). Adsorption isotherm experiments were conducted using various initial oil droplets concentrations (25–250 mg/L) at 35°C with a set amount of Fe_3O_4@GO@Ka nanocomposite (5 mg) for 60 min to assure emulsified oil droplets adsorption equilibrium on Fe_3O_4@GO@Ka nanocomposite. Samples centrifugation was carried out for 15 min at 3,500 rpm (Centurion Scientific C2 series centrifuges) for adsorbent separation from emulsion solution at the end of each experiment, and then the digital direct-reading turbidimeter (Orbeco–Hellige) was performed on 15 mL of the supernatant. The same process was used with emulsion blanks without any adsorbent.

2.9. Regeneration test

Because the Fe_3O_4@GO@Ka nanocomposite has been offered as an adsorbent for emulsified oil droplets removal from synthetic oil/water emulsion, it must be evaluated to see if it can be reused many times (Fig. 2). A simple

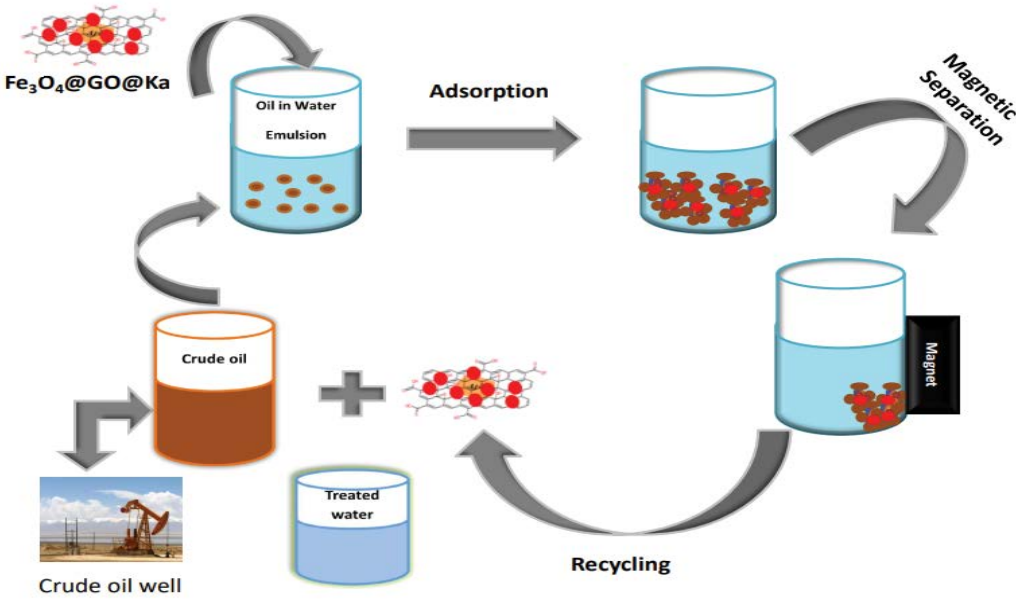

Fig. 2. Scheme of adsorption and recycling tests using Fe_3O_4@GO@Ka nanocomposite as an adsorbent.

solvent-washing approach was applied to regenerate the employed Fe_3O_4@GO@Ka nanocomposite. In this method, 0.005 g of utilized Fe_3O_4@GO@Ka nanocomposite was mixed with 25 mL of ethanol for 1 h at 35°C on a 350 rpm shaker water bath to desorb emulsified oil droplets from Fe_3O_4@GO@Ka nanocomposite. The regenerated Fe_3O_4@GO@Ka nanocomposite was employed in the following emulsified oil droplets adsorption experiments [12,23,71].

2.10. Adsorption capacity and removal efficiency

To estimate the amount of emulsified oil droplets removed by Fe_3O_4@GO@Ka nanocomposite, the adsorption capacity of emulsified oil, Q_t (mg/g), was computed by applying Eq. (1):

$$Q_t = \frac{\left(C_i - C_t\right) \times V}{W_a} \tag{1}$$

and the removal efficiency, R_t (%), was calculated using Eq. (2):

$$R_t = \left[\frac{\left(C_i - C_t\right)}{C_i}\right] \times 100 \tag{2}$$

where C_i represents the initial emulsified oil concentration (mg/L), C_t denotes the remaining concentration of emulsified oil at time t (mg/L), V is the volume of oil/water emulsion (mL), and W_a is the mass of Fe_3O_4@GO@Ka nanocomposite (mg). The adsorption capacity of Fe_3O_4@GO@Ka nanocomposite at equilibrium was expressed as Q_e (mg/g); when the concentration of emulsified oil reaches equilibrium (i.e., C_e, mg/L) [49].

2.11. Adsorption kinetics

The adsorption rate is investigated to create a quick and effective model. To investigate governing mechanisms of the adsorption process, including chemical reaction, diffusion control, and transfer of mass, the experimental data were analyzed using numerous kinetics models [46].

The pseudo-first-order (Lagergren model) and the pseudo-second-order models Eqs. (3) and (4) were used to assess the kinetic data of emulsified oil droplets adsorption [12].

$$\ln\left(Q_e - Q_t\right) = \ln Q_e - K_1 t \tag{3}$$

where Q_t and Q_e represent the amount of emulsified oil adsorbed on Fe_3O_4@GO@Ka nanocomposite (mg/g) at the reaction time t (min) and equilibrium time, respectively. K_1 (min^{-1}) refers to the pseudo-first-order rate constant [12]. The rate constant and Q_e are calculated by plotting the term $\ln(Q_e - Q_t)$ vs. t [49]. The manners of adsorption in solid–liquid systems were investigated using the Lagergren equation, in which a sole sorption site on the surface of (Fe_3O_4@GO@Ka) is supposed to be occupied by emulsified oil droplets [12,49].

$$\frac{t}{Q_t} = \frac{1}{K_2 Q_e^2} + \frac{t}{Q_e} \tag{4}$$

where K_2 (g/mg min) denotes the pseudo-second-order equation rate constant. The plot of t/Q_t against t is fitted with a linear fit, $1/Q_e$ represents the slope, while $1/K_2Q_e^2$ represents the intercept. The rate constant K_2 and Q_e are derived from the intercept and slope of the linear fit [49]. The emulsified oil is considered to be adsorbed to two sorption sites on the (Fe_3O_4@GO@Ka) surface when the pseudo-second-order equation is employed [12].

The intraparticle diffusion model was used to investigate the emulsified oil droplets diffusion behavior during the oil adsorption process as follows [2,12]:

$$Q_t = K_{p,i} t^{1/2} + C \tag{5}$$

where $K_{p,i}$ represents the constant of diffusion rate (mg/g $min^{1/2}$) at phase i and C (mg/g) is defined as the intercept.

The thickness of the boundary layer can be estimated using C values. If the intercept was larger, the surface sorption contribution in the rate-controlling step would be greater. Intraparticle diffusion is the single rate-limiting step for the adsorption process; if the Q_t vs. $t^{1/2}$ has a linear graph that goes across the origin [2,46].

2.12. Adsorption isotherms

Different models of adsorption isotherms are used to investigate the equilibrium adsorption capacity of emulsified oil droplets on Fe_3O_4@GO@Ka nanocomposite. The adsorption data were demonstrated using the Langmuir and Freundlich isotherm models [2,49]. To analyze the adsorption isotherm, the non-linear form of the Langmuir isotherm was initially used in the manner described in Eq. (6):

$$Q_e = \frac{Q_{\max} K_l C_e}{1 + K_l C_e} \tag{6}$$

The linearized equation is obtained by rearranging the above equation as follows:

$$\frac{C_e}{Q_e} = \frac{1}{Q_{\max}} C_e + \frac{1}{Q_{\max} K_l} \tag{7}$$

where Q_e represents the amount of emulsified oil droplets adsorbed at equilibrium on (Fe_3O_4@GO@Ka) surface (mg/g), C_e refers to the concentration of oil droplets at equilibrium (mg/L), $Q_{\max}$ is the Fe_3O_4@GO@Ka nanocomposite maximum adsorption capacity (mg/g) and K_l denotes a constant of Langmuir isotherm (L/mg).

The Langmuir constants K_l and $Q_{\max}$ (which are connected to the constant sorption free energy) can be calculated using the intercept and slope of a linear plotting of C_e/Q_e vs. C_e [2].

One of the most often used models for explaining adsorption behaviors and estimating maximal adsorption of solute is the Langmuir adsorption isotherm. This model assumes that monolayer adsorption occurs on a stable adsorbent surface that consists of a finite number of specific homogenous adsorption sites. Adsorption cannot be achieved on the same sites once occupied. As a result, when adsorbates fill all the adsorbent sites, a saturation of adsorption capacity is obtained [12,49,71].

The non-linear Freundlich isotherm is another model employed to analyze the adsorption isotherm data, as shown in Eq. (8):

$$Q_e = K_f C_e^{\frac{1}{n}} \tag{8}$$

where Q_e represents the adsorption capacity of Fe_3O_4@GO@Ka nanocomposite at the equilibrium (mg/g), K_f is the Freundlich isotherm constant, and C_e denotes the concentration of remaining emulsified oil when the system is at equilibrium, $1/n$ represents the adsorbent's heterogeneity factor, and n denotes the adsorption process's favorableness.

The adsorption is favorable ($0 < 1/n < 1$); the adsorption is unfavorable ($1/n < 1$); the adsorption is homogenous ($1/n = 1$) [37].

The following is a linearization of the previous equation:

$$\ln\left(Q_e\right) = \ln\left(K_f\right) + \frac{1}{n}\ln C_e \tag{9}$$

The Freundlich model doesn't predict the maximal adsorption capacity. It is an empirical formula that considers the adsorbent surface heterogeneity, the distribution of adsorption sites, and exponentially energies [2,49,71]. According to the Freundlich isotherm, Adsorbates adsorption takes place on adsorbents' heterogeneous surfaces, and that adsorption can take place in monolayer (chemisorption) or multilayer (physisorption) [12,71].

2.13. Thermodynamic parameters

Comprehending the adsorption process's nature depends on the numerical values of some thermodynamic parameters, namely Gibb's free energy change ($\Delta G°$), standard enthalpy change ($\Delta H°$), and standard entropy ($\Delta S°$). For the removal of oil droplets by Fe_3O_4@GO@Ka nanocomposite, these thermodynamic parameters were calculated using Eqs. (10) and (11) [12,23,37]:

$$\ln K_d = \frac{\Delta S°}{R} - \frac{\Delta H°}{RT} \tag{10}$$

$$\Delta G° = \Delta H° - T\Delta S° \tag{11}$$

where K_d represents the distribution constant of oil droplets between the solid phase and liquid phase at the equilibrium and calculated from Q_e/C_e. T is the adsorption temperature in Kelvin (K), and R denotes the universal gas constant (8.314 J/(mol·K)). The slope and intercept of the plot of $\ln K_d$ vs. $1/T$ (Van't Hoff plot) were used to determine $\Delta H°$ and $\Delta S°$, respectively [37].

3. Results and discussion

3.1. Characterization of nanocomposite

3.1.1. Fourier-transform infrared spectroscopy

The FT-IR spectra of kaolin, (GO@Ka), and Fe_3O_4@GO@Ka nanocomposite at the 4,000–400 cm^{-1} frequency range are shown in Fig. 3. FT-IR spectrum of kaolin shows strong absorption peaks at 3,690 cm^{-1}. The inner –OH stretching vibration is represented by the absorption bands 3,690 cm^{-1} [28,30,67]. Also, the amount of water physically absorbed on the clay's surface is represented by the band at 3,690 cm^{-1} [72]. The absorption band of the asymmetric stretching vibration of Si–O–Si and the telescoping vibration of O–Si–O was found at 1,699 cm^{-1} in the intermediate and low-frequency range. The Si–O stretching vibrations were ascribed to spectral bands at 1,006 cm^{-1} [28]. The bending vibration of the inner and surface hydroxyl groups of Al–OH are responsible for the bands between 790 and 909 cm^{-1} [28,30,67].

The FT-IR chart of GO@Ka was identical to that of kaolin, which indicate that kaolin was not eliminated and had a distributed role [28]. Furthermore, in the FT-IR spectrum of GO@Ka, numerous characteristic peaks appeared at 3,615; 1,699; 1,513; 1,394 and 1,051 cm^{-1}; these peaks were assigned to the stretching vibrations of hydroxyl groups (–OH), carboxyl groups (–COOH), C=C groups, epoxide (–O–), and alkoxy groups (C–O–C) indicating the successful formation of GO [28,37,50,65].

In the FT-IR spectrum of Fe_3O_4@GO@Ka nanocomposite, two prominent absorption bands at roughly 464 and 781 cm^{-1} were appeared, indicating the presence of magnetic nanoparticles [67]. The shifts of COOH band, from 1,699 to 1,624 cm^{-1}, and of C=C band, from 1,513 to 1,509 cm^{-1}, suggest the incorporation of Fe_3O_4 NPs into the functional groups of GO [23]. The decorating of Fe^{2+}, Fe^{3+} ions connected with high electronegativity sites on the GO surface (OH, C=O, and COOH groups) is shown by a decrease in the intensity of oscillations at 1,699; 1,513 and 1,051 cm^{-1} in Fe_3O_4@GO@Ka nanocomposite spectrum [65].

3.1.2. XRD patterns

The XRD patterns of the Fe_3O_4@GO@Ka nanocomposite are depicted in Fig. 4. Various peaks in the XRD pattern of Fe_3O_4@GO@Ka nanocomposites at $2\theta = 26.53°$, 36.44°, 42.37°, 54.93°, 59.87°, and 68.61° were ascribed to (220), (311), (400), (422), (511), and (440), crystallographic planes. These peaks matched the crystallographic properties of Fe_3O_4 NPs quite well [50,65]. Peaks at 2θ of 12.3°, 20.8°, 25.2°, 26.6°, and 55° indicate the presence of kaolinite [67].

The sharp and intense peaks that appeared at the $2\theta = 12.3°$ and 26.6° in kaolin represent the typical diffraction peak associated with kaolinite. Those peaks were less intense (especially at 26.6°) in the XRD patterns of Fe_3O_4@GO@Ka nanocomposite implying a decrease in the clays' crystallinity [30].

The disappearance of GO peak at $2\theta = 11.12°$ in GO@Ka and Fe_3O_4@GO@Ka nanocomposite diffraction patterns is attributed to the formation of more single-layer graphene oxide, resulting in a weak carbon diffraction peak [73]. The spacing between GO sheets was calculated to be 0.795 nm using the $2\theta = 11.12°$ diffraction peak assigned to the (002) crystallographic planes [50,65,73].

3.1.3. Scanning electron microscopy

Fig. 5 illustrates the morphology of kaolin, GO@Ka, and Fe_3O_4@GO@Ka nanocomposite. Kaolin has a porous surface with a layer structure, as seen in Fig. 5a. In the SEM

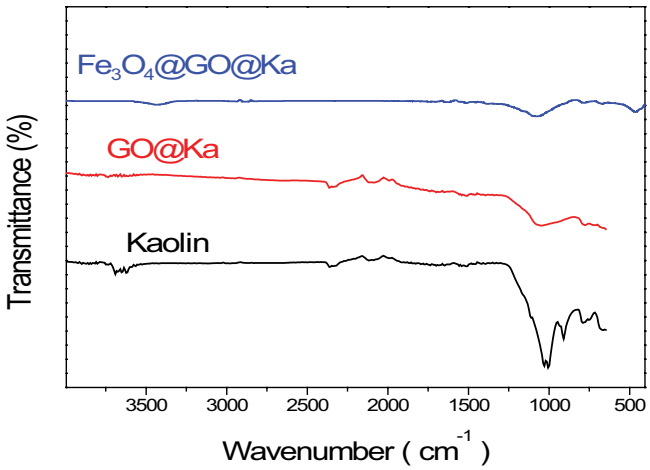

Fig. 3. FT-IR spectra of kaolin, GO@Ka, and Fe_3O_4@GO@Ka nanocomposite.

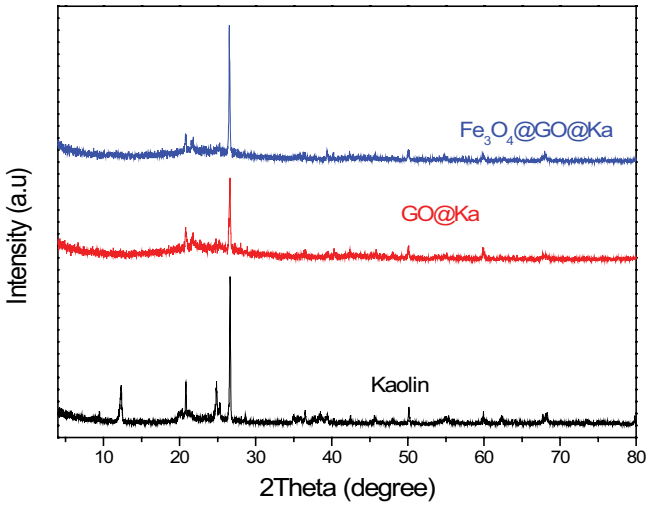

Fig. 4. XRD spectra of kaolin, GO@Ka, and Fe_3O_4@GO@Ka nanocomposite.

morphology of GO@Ka Fig. 5b, small clusters of graphene oxide sheets were seen. The kaolin flakes were wrapped in GO sheets, as illustrated in Fig. 5b, suggesting that the GO-kaolin samples were successfully prepared [37]. The formation of numerous wrinkles in the structure of GO indicates the presence of oxygen-containing functional groups. High-energy adsorption sites are thought to be these wrinkles [39]. The SEM pictures of the Fe_3O_4@GO@Ka nanocomposite in Fig. 5c reveal that iron oxide particles decorated the rough surface of GO@Ka. The development of an unlimited pores number on the uneven surface of composite increases the surface area and makes adsorption easier. The increased surface area provides more binding sites for iron oxide particles [72,74].

3.1.4. High-resolution transmission electron microscopy

Fig. 6 shows the HR-TEM pictures of kaolin, GO@Ka, and Fe_3O_4@GO@Ka nanocomposite. The flaky graphene oxide nanosheets were used to cover kaolin flakes, as shown in Fig. 6b, where GO was made up of thin, translucent layers with wrinkles on the surface of the GO nanosheet, which indicated the presence of oxygen-containing groups on the GO [39]. Also, Fig. 6b shows that the modified kaolin particles are inclined to agglomerate, creating hierarchical micro- and nanoscale structures. It is worthwhile to mention that the surface roughness will be improved by the hierarchical structures [33]. In Fig. 6c, the flake structure of GO provided an excellent plate form for iron oxide loading, where Fig. 6c illustrates that iron oxide nanoparticles were anchored to the graphene surface and piled on GO nanosheets drapes and flaws [23,28].

3.1.5. Brunauer–Emmett–Teller

The prepared Fe_3O_4@GO@Ka nanocomposite has a surface area of 249.3 m^2/g with a total pore volume of 0.1952 cm^3/g and a mean pore diameter of 1.749 nm which was larger than that of kaolin 8.337 m^2/g indicating that GO has the potential to increase the specific surface area of kaolin, as well as improve the dispersed state of iron nanoparticles [28]. Table 1 the large pore volume and surface area of the Fe_3O_4@GO@Ka nanocomposite suggest that this adsorbent will have a high adsorption capacity [26]. The decrease of Fe_3O_4@GO@Ka nanocomposite mean pore diameter demonstrated that the Fe_3O_4 NPs occupied parts of the kaolin pores during the modification process [75].

3.1.6. Vibrating-sample magnetometer

In order to explore the magnetic properties of bare Fe_3O_4 and Fe_3O_4@GO@Ka nanocomposite, VSM was employed to record the magnetization values of these materials at 308K. Both the naked Fe_3O_4 NPs and the Fe_3O_4@GO@Ka nanocomposite exhibit magnetic properties with no remanence or coercitivity, as illustrated in Fig. 7. For the naked Fe_3O_4 NPs and the Fe_3O_4@GO@Ka nanocomposite, the saturation magnetization (MS) was determined to be 60 and 20 emu/g, respectively. In this way, the diamagnetic kaolin in the Fe_3O_4@GO@Ka nanocomposite is responsible for lowering the magnetization value. Furthermore, those magnetization values are much lower than those of bulk Fe_3O_4 (MS ~ 80 emu/g) [47,65].

3.2. Batch adsorption studies

3.2.1. Effect of contact time

To establish the optimum contact time required for the adsorption process of emulsified oil droplets to attain equilibrium, adsorption studies were done at various periods ranging from 0 to 60 min. The removal of emulsified oil droplets using Fe_3O_4@GO@Ka nanocomposite increases rapidly in the first 5 min until reach its equilibrium time at 10min with a removal efficiency of 72.47%. After that, the removal of emulsified oil droplets increases slowly until reaching its maximum at 60 min with a removal efficiency of 75.14%, as illustrated in Fig. 8. This implies that the kinetic nature of the adsorption process involves two stages. The fast removal rate stage until reach equilibrium, then the

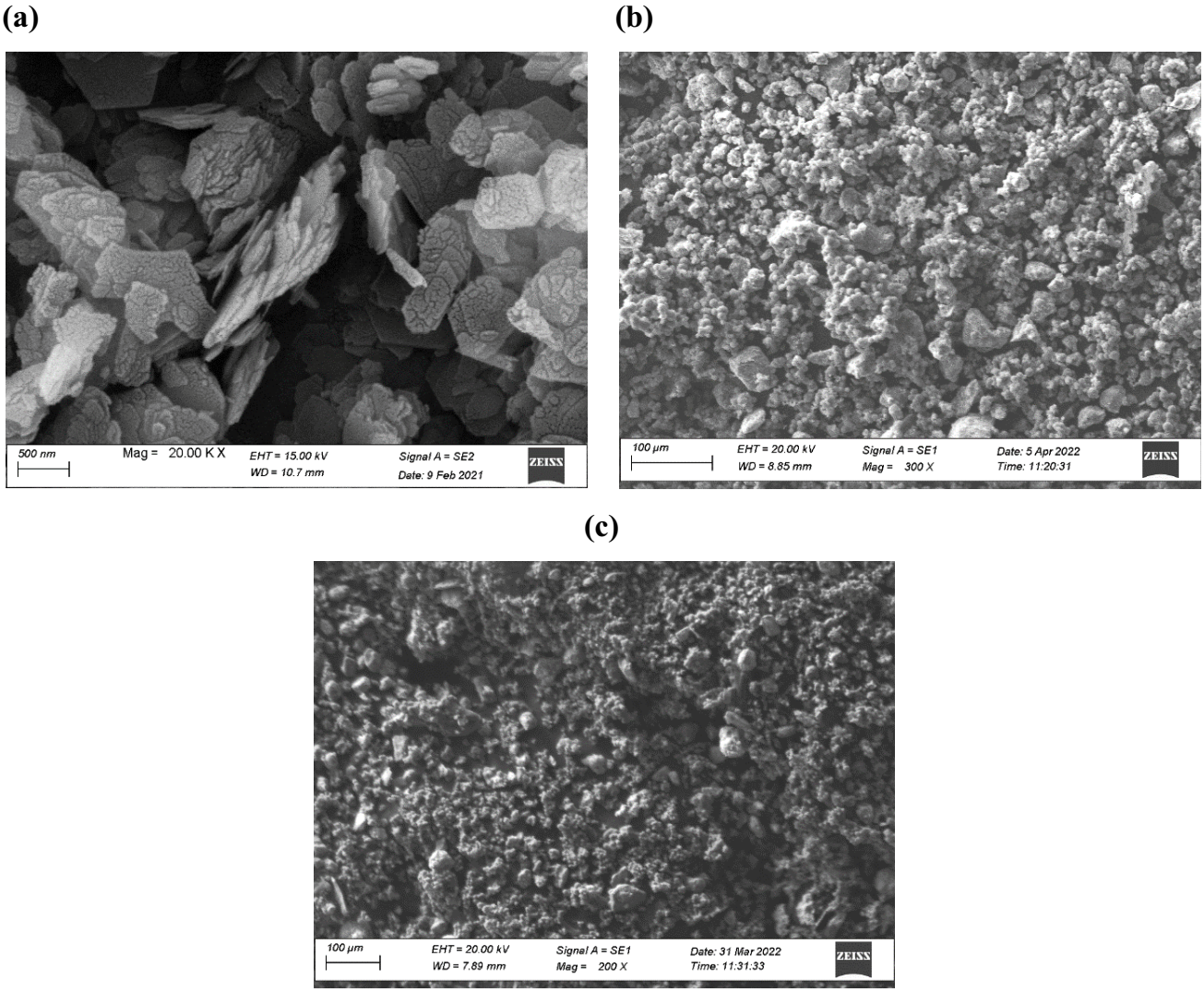

Fig. 5. SEM images of kaolin (a), GO@Ka (b), and Fe_3O_4@GO@Ka nanocomposite (c).

Table 1
BET of kaolin, GO@Ka, and Fe_3O_4@GO@Ka nanocomposite

Composites	Surface area (m^2/g)	Total pore volume (cm^3/g)	Mean pore diameter (nm)
Kaolin	8.337	0.07686	36.87
GO@Ka	332.2	0.1696	2.041
Fe_3O_4@GO@Ka	249.3	0.1952	1.749

gradual slow removal rate stage of emulsified oil droplets before reaching the maximum [49,71].

The presence of a great number of vacant active sites on the Fe_3O_4@GO@Ka nanocomposite surface is attributed to the quick emulsified oil droplets uptake rate at the start of the adsorption stage; however, as time passes, these active sites gradually decrease due to their occupation by oil, until they are completely saturated by emulsified oil droplets, causing no additional emulsified oil adsorption. Due to the development of repulsive force between the (Fe_3O_4@GO@Ka) nanocomposite and the emulsified oil droplets [2,49,68,71]. The maximum contact time for emulsified oil droplets removal was achieved at around 60 min, with a removal efficiency of 75.14% and adsorption capacity of 93.93 mg/g.

3.2.2. Effect of pH

The pH value is an essential parameter that affects the stability of oil/water emulsions and, therefore, influences the adsorption process of emulsified oil droplets to Fe_3O_4@

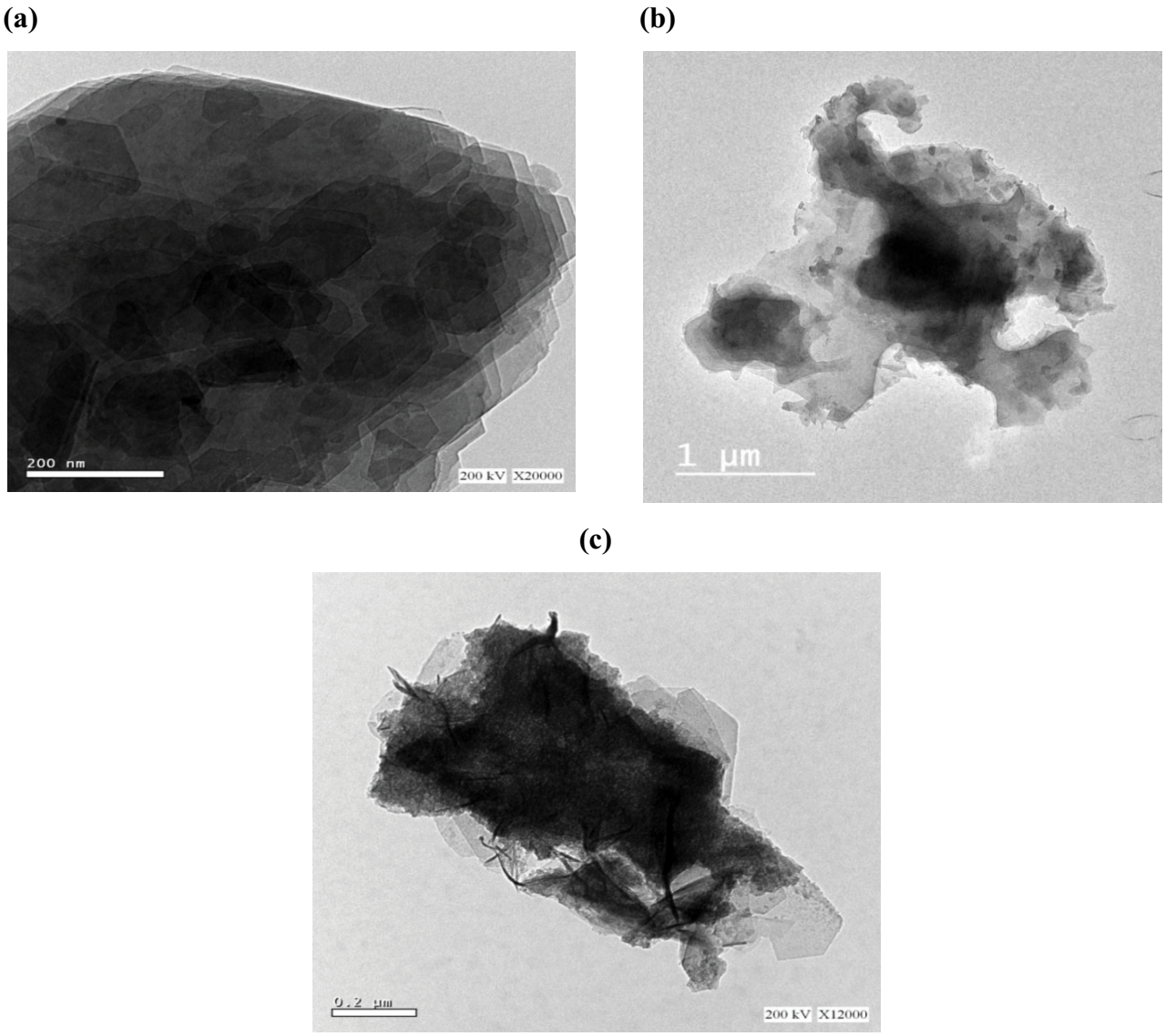

Fig. 6. HR-TEM images of kaolin (a), GO@Ka (b), and Fe_3O_4@GO@Ka nanocomposite (c).

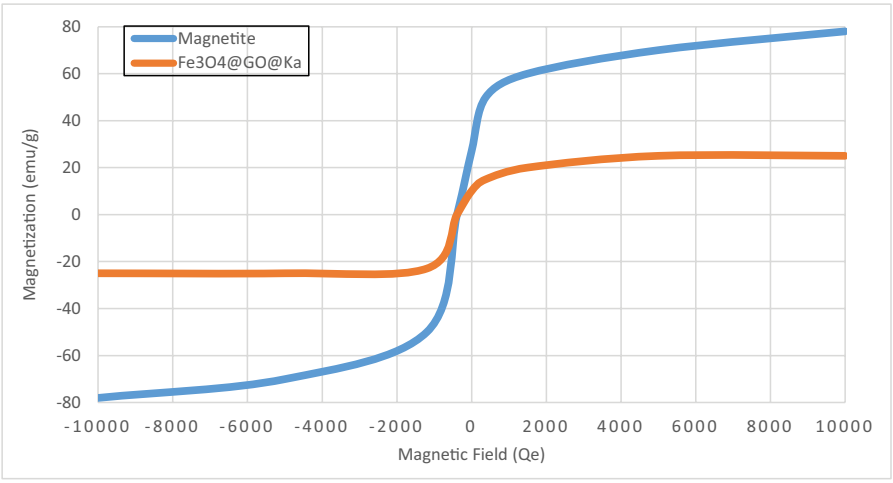

Fig. 7. VSM analysis for the magnetite (Fe_3O_4 NPs) and Fe_3O_4@GO@Ka nanocomposite.

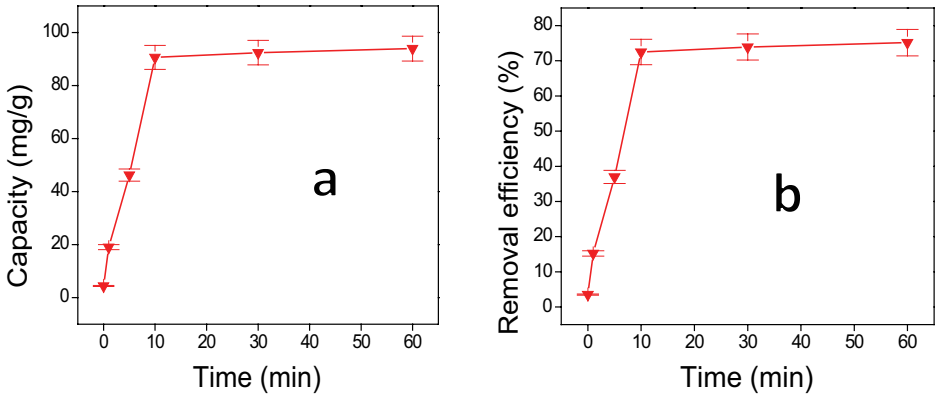

Fig. 8. The influence of contact time on the adsorption capacity (a) and on the removal efficiency (b) of emulsified oil droplets by Fe_3O_4@GO@Ka (C_o = 25.0 mg/L, composite amount = 5.0 mg, pH = 7.0, T = 35°C).

GO@Ka nanocomposite [12,71,76]. The pH of the emulsion was changed from 2 to 11 to explore the pH influence on the removal efficiency of emulsified oil droplets. Fig. 9 depicts the impact of emulsion solution pH on emulsified oil droplets removal efficiency by Fe_3O_4@GO@Ka nanocomposite.

Fig. 9 shows an increase in the removal efficiency with rising the pH until reaching its maximum value of about 92.72% at pH 7. After that, the percentage removal gradually falls when the pH of the solution rises under alkaline circumstances at pH above 7. This finding implies that both acidic and alkaline environments are ineffective, and pH 7 was the optimal pH for elimination. The same thing was observed by a large number of researchers [12,76]. This was explained by the pore structure of the joint reed surface being easily penetrated by emulsified oil droplets molecules under acidic conditions. In contrast, under alkaline conditions (pH greater than 7), hydroxyl ions may accumulate on the Fe_3O_4@GO@Ka nanocomposite surface; consequently, the electrostatic repulsion among oil droplets and the Fe_3O_4@GO@Ka nanocomposite has risen [12,46,76].

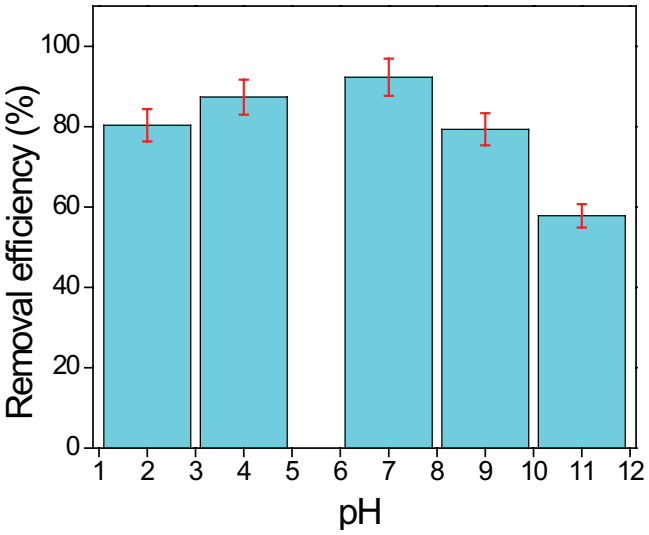

Fig. 9. The influence of pH on removal efficiency of emulsified oil droplets by Fe_3O_4@GO@Ka (C_o = 25.0 mg/L, composite amount = 5.0 mg, time = 60.0 min, T = 35°C).

3.2.3. *Effect of the initial concentration of emulsified oil*

The influence of initial concentrations of crude oil (C_o = 25–250 mg/L) on the oil adsorption capacity and the removal efficiency of Fe_3O_4@GO@Ka nanocomposite for emulsified oil droplets was investigated at the optimum time (1 h). Fig. 10 shows that the adsorption capacity (Q_e) of oil to Fe_3O_4@GO@Ka nanocomposite rises from 116.3 to 1,148 mg/g, and the removal efficiency declines from 93.06% to 91.90%, as the initial concentration of emulsified oil droplets increases from 25 to 250 mg/L. These findings point to that emulsified oil droplet's adsorption process based on the initial concentration of emulsified oil droplets. The initial concentration supplies the principal driving force (acts as a powerful propellant) to overcome all impedances in the mass transfer of the emulsified oil droplets among the oil/water emulsion and adsorbent [46,68]. Not sufficient time is provided for adsorption at high initial emulsified oil concentration, so the adsorption capacity is lower hence removal efficiency decreases attributed to, at a low initial emulsified oil concentration, the removal efficiency of Fe_3O_4@GO@Ka nanocomposite for emulsified oil droplets is higher since the adsorption process is slow; this is the reason that illustrated. Also, because increasing emulsified oil droplets concentration increase the competition for the active sites on the Fe_3O_4@GO@Ka nanocomposite and this will lead to the saturation of active sites at higher concentration, so the adsorption efficiency diminishes [37,68].

3.2.4. *Effect of composite quantity*

Fe_3O_4@GO@Ka nanocomposite quantity ranged from 1 to 9 mg to ascertain the impact of composite amount on the adsorption capacity and the removal efficiency of (Fe_3O_4@GO@Ka) for oil droplets. Fig. 11 depicts the influence of Fe_3O_4@GO@Ka nanocomposite quantity on emulsified oil droplets removal efficiency. From the findings seen in Fig. 11, as the Fe_3O_4@GO@Ka nanocomposite quantity grew from 1 to 5 mg, the removal efficiency of crude oil droplets rose significantly from 81.95% to 86.35%. After that, as the

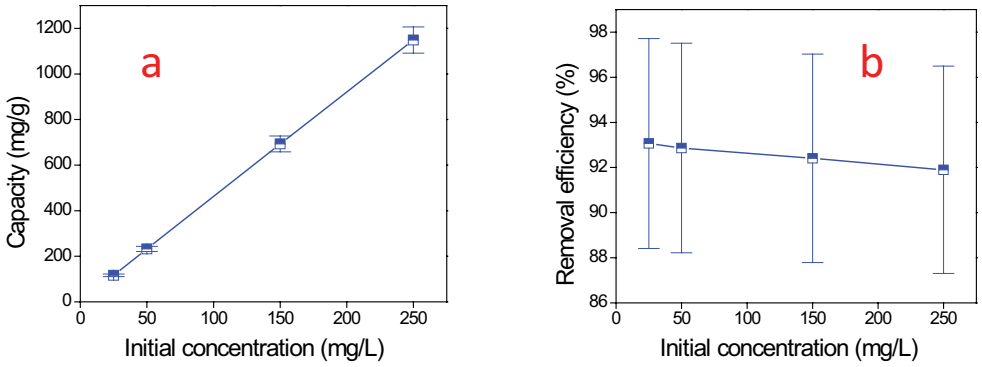

Fig. 10. The influence of initial emulsified oil concentration on the adsorption capacity (a) and the removal efficiency (b) of Fe_3O_4@GO@Ka for emulsified oil droplets (time = 60.0 min, composite amount = 5.0 mg, pH = 7.0, T = 35°C).

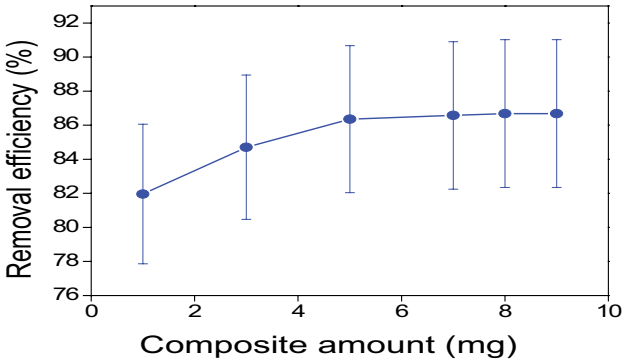

Fig. 11. The influence of composite amount on the removal efficiency of Fe_3O_4@GO@Ka for emulsified oil droplets (C_o = 25.0 mg/L, time = 60.0 min, pH = 7.0, T = 35°C).

Fe_3O_4@GO@Ka nanocomposite quantity grew from 5 to 9 mg, there was no significant change in the removal efficiency. As a result, 5mg of Fe_3O_4@GO@Ka nanocomposite was chosen as the optimal dose. This behavior can be explained by the fact that by increasing the weight of the adsorbent, the number of accessible adsorption sites also increase [76].

3.2.5. Effect of temperature

The influence of emulsion temperature on removal efficiency and adsorption capacity was examined at temperatures ranging from 25°C to 60°C and 25 mg/L initial concentration of emulsified oil. As illustrated in Fig. 12, as the temperature rose from 25°C to 35°C. The adsorption capacity increased from 67.46 to 123.5 mg/g and removal efficiency of emulsified oil droplets increased from 53.97% to 98.80% until reach its maximum of 99.94% at 50°C, demonstrating that the adsorption reaction of emulsified oil droplets onto Fe_3O_4@GO@Ka nanocomposite is endothermic. The fact that adsorption capacity increased with temperature suggested that emulsified oil droplets' adsorption by Fe_3O_4@GO@Ka nanocomposite might entail physical and chemical sorption. The increased number of adsorption sites generated by bond rupture could explain this impact [46].

3.3. Adsorption kinetic studies

To evaluate the time-dependent adsorption data, the most common adsorption kinetic models, including, the pseudo-first-order (Lagergren model), pseudo-second-order kinetic models, and the intraparticle diffusion models were employed [49]. Fig. 13a–c show linearized graphs of the three models. Table 2 lists the fitting correlation coefficients and the derivative kinetic parameters of the three models. As shown in Table 2, the correlation coefficient (R^2) obtained from the fit of the pseudo-second-order kinetic model is also 0.9921, which is significantly higher than the correlation coefficient produced from the pseudo-first-order kinetics model fit in Table 2. Oil droplet adsorption followed pseudo-second-order kinetics based on the high correlation coefficients and excellent agreement between models fit and empirically observed equilibrium adsorption turnover.

The pseudo-second-order kinetic model generally posits that chemical adsorption, which includes covalent forces among the Fe_3O_4@GO@Ka nanocomposite and emulsified oil droplets or coordination bond, is the rate-limiting phase [37,49]. As a result, the uptake process of emulsified oil droplets on Fe_3O_4@GO@Ka nanocomposite could be deduced as chemisorption.

Although laws of pseudo-first-order rate and pseudo-second-order rate can be utilized to assess kinetic results, they do not give information on oil adsorption diffusion. As a result, the model of intraparticle diffusion Eq. (5) was applied to examine the experimental kinetic data [12].

The uptake curve should be linear if the intraparticle diffusion is twisted throughout the adsorption phase. If these lines cross through the origin, the intraparticle diffusion is the rate governing step [46,49]. It can be seen that Q_t vs. $t^{1/2}$ curve, does not pass across the origin, this indicates that the rate-limiting step was not the intraparticle diffusion.

Also, because the R^2 value is significantly less than that of the pseudo-second-order kinetic model Table 2, the mechanism of oil uptake is not represent the intraparticle diffusion. This result was expected because the majority of processes of intraparticle diffusion require numerous hours to achieve stability. Because hydrocarbon oil molecules lack the groups of chemisorption, bonding of oil molecules to adsorbent is most likely mediated by London Π bonding or van der Waals forces and the nanoparticles'

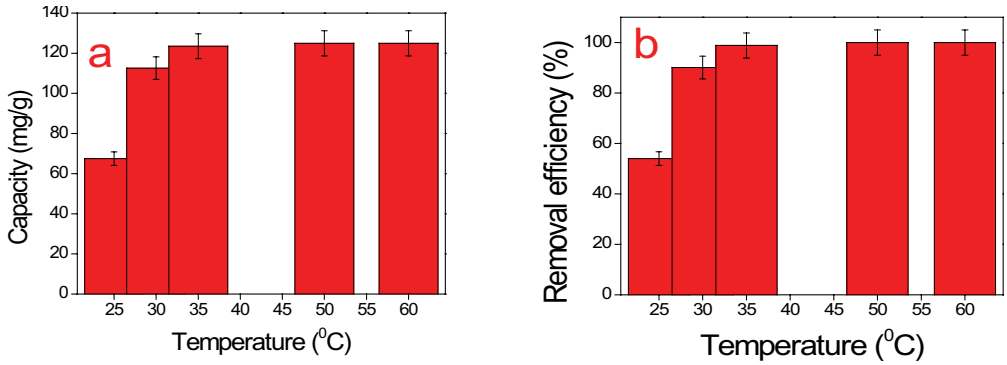

Fig. 12. The influence of temperature on the adsorption capacity (a) and the removal efficiency (b) of Fe_3O_4@GO@Ka for emulsified oil droplets (C_o = 25.0 mg/L, time = 60.0 min, composite amount = 5.0 mg, pH = 7.0).

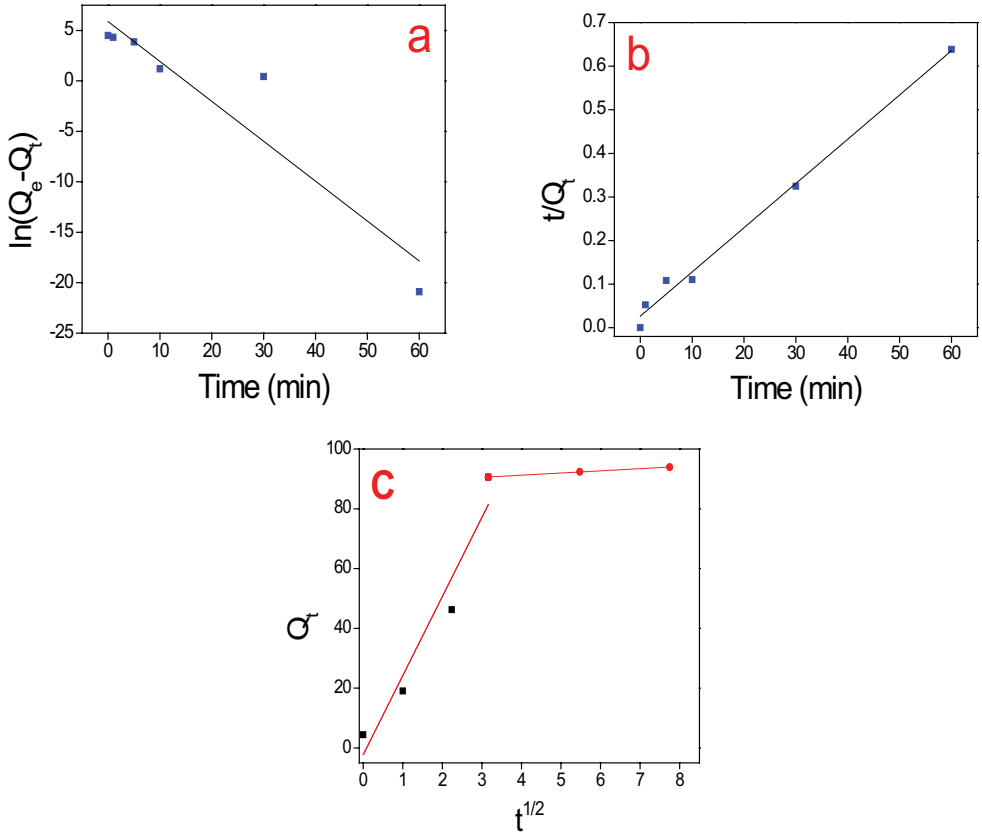

Fig. 13. Adsorption kinetic models, pseudo-first-order (a), pseudo-second-order (b), and intraparticle diffusion (c), of emulsified oil droplets adsorption on Fe_3O_4@GO@Ka.

well-known high surface potential is most likely to blame for the incredible rapidity of oil uptake [10,49].

3.4. Adsorption isotherm models

The maximal adsorption capacity of the Fe_3O_4@GO@Ka nanocomposite was determined using equilibrium adsorption data. Fig. 14a and b show the oil adsorption capacity of Fe_3O_4@GO@Ka nanocomposite as a function of the equilibrium concentration in an aqueous solution. To explain the interaction of oil droplets and Fe_3O_4@GO@Ka nanocomposite surface, two typical forms of isotherms, Langmuir and Freundlich isotherm models, were used. Fig. 14a and b depict the curves for the two fitted isotherm models.

Table 3 lists the computed values for the parameters of Freundlich and Langmuir models, in addition to the correlation coefficient (R^2) values of the two isotherms.

Fig. 14a and b show that Freundlich strongly agrees with the experimental findings. R^2 values for Freundlich is 0.9998. As indicated by the correlation coefficient (R^2) of Fe_3O_4@GO@

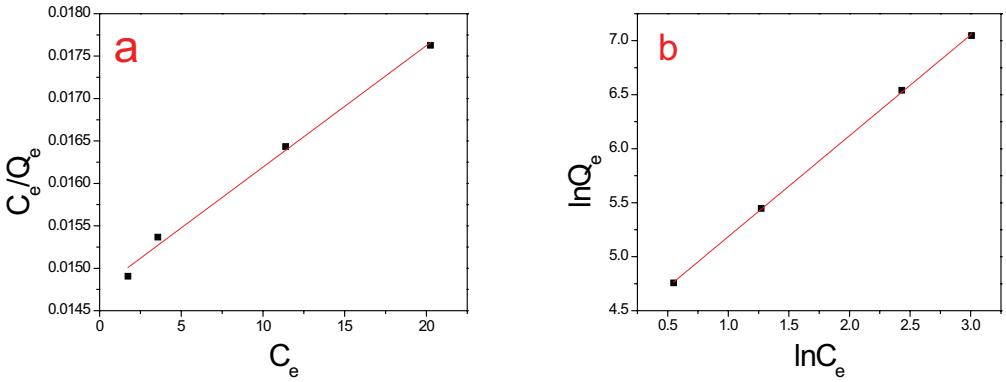

Fig. 14. Adsorption isotherm models, Langmuir isotherm (a) and Freundlich isotherm (b), of emulsified oil droplets adsorption on Fe_3O_4@GO@Ka.

Table 2
Adsorption kinetics parameters for emulsified oil droplets adsorption to Fe_3O_4@GO@Ka

Models	Parameters	Values
	R^2	0.8881
Pseudo-first-order	K_1 (min^{-1})	0.3956
	Q_e (mg/g)	361.2
	R^2	0.9921
Pseudo-second-order	K_2 (g/mg min)	0.00394
	Q_e (mg/g)	98.03
	R^2	0.9679
Intraparticle diffusion	K_p ($mg/g\ min^{1/2}$)	13.58
	C (mg/g)	43.04

Table 3
Adsorption isotherm constants for emulsified oil droplets adsorption to Fe_3O_4@GO@Ka

Models	Parameters	Values
	Q_{max} (mg/g)	10000
Langmuir isotherm	K_l (L/mg)	0.0068
	R^2	0.9949
	n	1.070
Freundlich isotherm	K_f (L/mg)	70.22
	R^2	0.9998

Table 4
Thermodynamic parameters for emulsified oil droplets adsorption on Fe_3O_4@GO@Ka nanocomposite

Temperature (K)	ΔG (kJ/mol)	ΔH (kJ/mol)	ΔS (kJ/mol·K)
298	–6.664		
303	–9.731		
308	–12.80	176.2	0.6134
323	–21.10		
333	–28.13		

Ka, Freundlich isotherm models represented the emulsified oil droplets' adsorption onto Fe_3O_4@GO@Ka nanocomposite better than Langmuir isotherm. The adsorption data's fit to the Freundlich isotherm suggests that adsorption of oil droplets by Fe_3O_4@GO@Ka nanocomposite is multilayer adsorption that can occur on heterogeneous surfaces [46,76].

As a result, the total amount of emulsified oil droplets adsorbed on Fe_3O_4@GO@Ka nanocomposite equals the sum of adsorption on all sites, with the higher energy binding sites occupied first until the adsorption energies exponentially declined after the adsorption process was completed [2,49]. The value of n (n = 1.070) shown in Table 3 suggests that oil droplets uptake onto Fe_3O_4@GO@Ka nanocomposite is favorable.

3.5. Thermodynamic parameters

The thermodynamic parameters' values are presented in Table 4, which shows Gibb's free energy ($\Delta G°$) for emulsified oil droplets uptake by Fe_3O_4@GO@Ka nanocomposite at various temperatures (298, 303, 308, 323, and 333 K). Table 4 shows that the values of $\Delta G°$ fell as the temperature rose. At all temperatures, the values of $\Delta G°$ were negative, confirming the process is viable and that oil droplets adsorption occurs spontaneously. The fact that the absolute value of $\Delta G°$ decreases as temperature rises (the $\Delta G°$ became more negative) shows that emulsified oil droplets' affinity for Fe_3O_4@GO@Ka nanocomposite is more favorable at higher temperatures [12]. $\Delta H°$, and $\Delta S°$ were calculated using the slope and intercept of the $\Delta G°$ against the T plot, which is also provided in Table 4. The positive $\Delta H°$ values were evidence of the endothermic character of oil adsorption to Fe_3O_4@GO@Ka nanocomposite. The positive $\Delta S°$ indicates that emulsified oil droplets and Fe_3O_4@GO@Ka nanocomposite exhibit a significant attraction to one other. The positive $\Delta S°$ readings also indicated that during the adsorption process, the degrees of randomness at the solid-solution interface were growing [12,37,46]. The aforementioned thermodynamic metrics revealed that adding GO to raw kaolin improved adsorption performance [37].

3.6. Regeneration test

Although Fe_3O_4@GO@Ka nanocomposite is a low-cost adsorbent, it is nevertheless necessary to assess its recyclability in emulsified oil droplets adsorption to gain insight into the process's subsequent design and optimization. A washing technique by ethanol was used to renew it for emulsified oil droplets removal from Fe_3O_4@GO@Ka nanocomposite [12,77]. The removal efficiency of oil droplets using Fe_3O_4@GO@Ka nanocomposite after numerous regeneration cycles is shown in Fig. 15. The oil droplets removal efficiency of the sample was measured after each cycle. The results reveal that, even after four cycles of recycling, the efficiencies of the recycled Fe_3O_4@GO@Ka nanocomposite for removing emulsified oil droplets are not significantly decreased compared to those of the fresh ones. That suggests the effectiveness of the ethanol-washing method in regenerating the Fe_3O_4@GO@Ka nanocomposite. Thus, it may be recycled several times without noticeably diminishing its adsorption capacity.

3.7. Adsorption mechanism of emulsified oil droplets on Fe_3O_4@GO@Ka nanocomposite

Fig. 16 illustrates the schematic of emulsified oil droplets adsorption mechanism of Fe_3O_4@GO@Ka nanocomposite. GO which is rich in functional groups (e.g., –OH, –COOH) may interact with kaolin by two methods: the first it can interact with the surface functional groups of kaolinite via hydrogen bond [78]. The second-way it can interact with positively charged at the alumina face via electrostatic interaction [79]. To enhance dispersion and inhibit agglomeration, resulting in kaolinite exfoliation and the formation of GO@Ka homogenous composite [78]. The surfactant plays an important role in stabilizing oil droplets. The surfactant molecules, which are sodium dodecyl sulfate (SDS), might be adsorbed on the oil/water interface and produce a negatively charged protective interfacial layer, which functions as a physical barrier to prevent the emulsified oil droplets from coalescing during the emulsifying process [23]. The addition of Fe_3O_4 NPs to the negative surfaces of GO has a significant influence on the stability of the oil emulsion breaking process, resulting in a significant increase in oil adsorption capacity on the GO surface. The presence of Fe^{3+} on the surfaces of GO will change the characteristics of the liquid/liquid and liquid/air interfaces. Fe^{3+}, for example, lowers

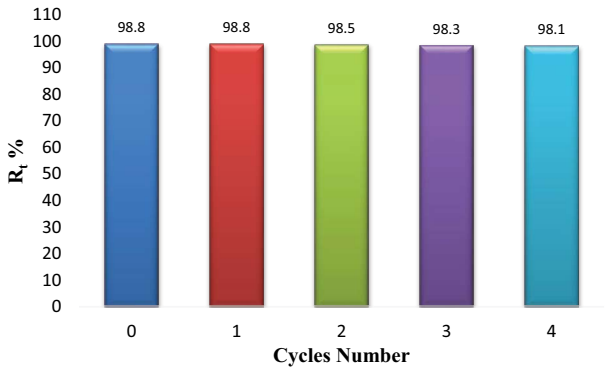

Fig. 15. Recyclability of Fe_3O_4@GO@Ka for oil droplets adsorption (time = 60.0 min, pH = 7.0, C_o = 25.0 mg/L, composite amount = 5.0 mg, T = 35°C).

Table 5
Removal efficiencies of various adsorbents for emulsified oil droplets removed from different oil/water emulsions

Adsorbent	Type of oil emulsion	Initial oil concentration (mg/L)	Adsorbent dose (g)	Adsorption equilibrium time (min)	Removal efficiency (%)	References
Thermally reduced graphene (TRG)	Diesel fuel/water emulsion	100	0.003	10	55%	[49]
Graphene nanoplatelets (GNP)	Diesel fuel/water emulsion	100	0.003	10	48%	[49]
Graphene oxide	Diesel fuel/water emulsion	100	0.003	10	62%	[10]
Amorphous carbon thin film (ACTF)	Egyptian condensate oil/water emulsion	100	5.0	360	93.3%	[68]
Zeolitic imidazolate framework (ZIF-8)	Soybean oil/water emulsion	450	0.002	100	66.7%	[71]
Ferric oxide nanoparticles doped carbon nanotubes	Gasoline oil/water emulsion	841	0.02	15	98.5%	[2]
Feldspar-banana peel biochar composite (FBPC)	Estuary crude oil/water emulsion	7500	0.3	120	56%	[21]
	Yokri crude oil/water emulsion	7500	0.3	90	97%	[21]
Fe_3O_4@GO@Ka nanocomposite	Crude oil/water emulsion	25	0.005	60	98.8%	This study

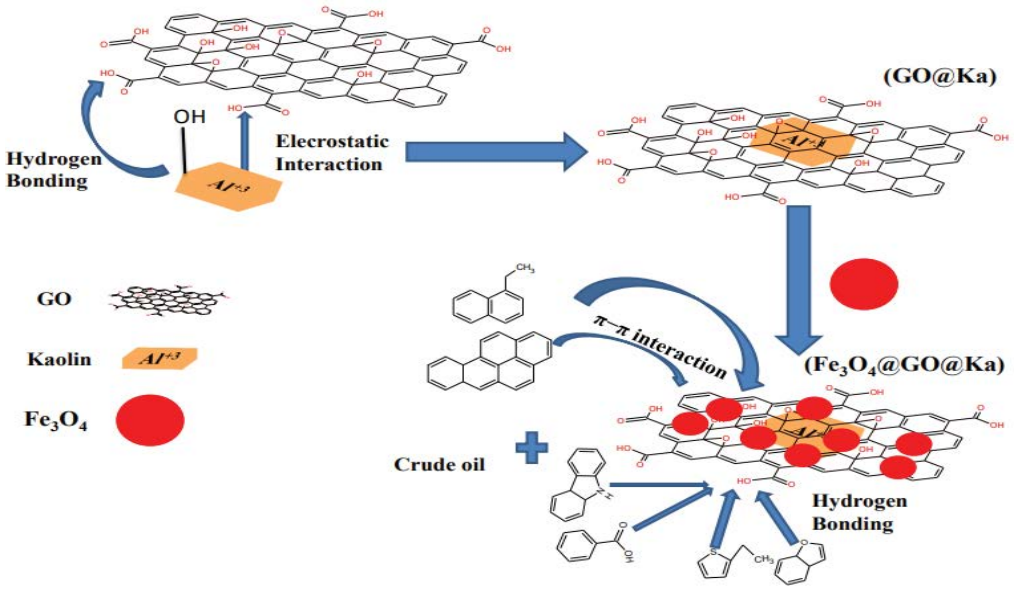

Fig. 16. Illustrate the mechanism of emulsified oil droplets removal by Fe_3O_4@GO@Ka nanocomposite.

the interfacial tension between the dispersed oil phase and the water and then raises it between the air bubbler and the oil phase. As a result, coating GO with Fe_3O_4 NPs increases oil droplet coalescence, which should improve oil adsorption absorption [2]. The benzene ring in oil molecules can connect with Fe_3O_4@GO@Ka nanocomposite via π–π interaction because hydrocarbon oil molecules lack accepted manuscript chemisorption groups [49,78].

3.8. Comparison of the Fe_3O_4@GO@Ka adsorption behavior with other studies

In this investigation, we compared the emulsified oil adsorption removal efficiency of the Fe_3O_4@GO@Ka nanocomposite utilized in this study to the removal efficiencies of other published adsorbents such as graphene oxide, zeolitic imidazolate framework (ZIF-8), feldspar-banana peel biochar composite (FBPC), and others. This comparison showed that Fe_3O_4@GO@Ka nanocomposite performed better and had a greater adsorption capacity than other adsorbents, as shown in Table 5. This is attributed to the graphene oxide-based materials have distinctive physical and chemical characteristics such as high specific surface area and pore volume.

4. Conclusion

In this paper, the Fe_3O_4@GO@Ka nanocomposite was successfully synthesized by a simple approach and utilized in oil droplet removal from oil/water emulsions. The introduction of GO into kaolin result in increasing the surface area as well as the number of active binding sites, which in turn, will increase the adsorption efficiency of the prepared nanocomposite. The influence of contact time, pH of emulsion, initial emulsified oil concentration, composite quantity, and temperature on emulsified oil droplet adsorption on Fe_3O_4@GO@Ka nanocomposite was investigated using a batch method to identify the best circumstances. At higher temperatures, Fe_3O_4@GO@Ka nanocomposite adsorption capacity was enhanced. The highest emulsified oil adsorption was achieved at a pH of 7, whereas acidic and alkaline conditions make it difficult for Fe_3O_4@GO@Ka nanocomposite to adsorb emulsified oil. The Langmuir and Freundlich isotherm models were used to examine the equilibrium isotherm data and it was found that the adsorption data match the Freundlich isotherm well. The emulsified oil droplets adsorption kinetics were explored using three distinct models (pseudo-first-order, pseudo-second-order, and intraparticle diffusion). The pseudo-second-order sorption kinetics model best correlated with the oil droplets adsorption to Fe_3O_4@GO@Ka nanocomposite. According to the thermodynamic study, the emulsified oil droplets adsorption to Fe_3O_4@GO@Ka nanocomposite was endothermic and spontaneous. Following a simple ethanol washing process, Fe_3O_4@GO@Ka nanocomposite was shown to be reused for several cycles. Because of its competitive adsorption capacity and reusability, the Fe_3O_4@GO@Ka nanocomposite might be considered an outstanding adsorbent for the removal of emulsified oil droplets from oil/water emulsions.

References

[1] H. Gul Zaman, L. Baloo, R. Pendyala, Application in the optimization of Pb(II) adsorption by chitosan from produced water by using response surface methodology, Int. J. Environ. Sci. Technol., (2022) 1–12, doi: 10.1007/s13762-022-03927-0.
[2] A.E. Abbas, M.A. Kassab, I. El-Gamal, B.M. Shawky, M. Fathy, R. Hosny, Study for estimating the effective way for managing the produced water, Int. J. Chem. Sci., 17 (2019) 309.
[3] H.H. El-Maghrabi, R. Hosny, M. Ramzi, M. Fathy, Novel mesoporous silica (MCM-41) and its characterization for oil adsorption from produced water injected in water injection projects using fixed bed column processes, Desal. Water Treat., 60 (2017) 70–77.
[4] B. Peng, Z. Yao, X. Wang, M. Crombeen, D.G. Sweeney, K.C. Tam, Cellulose-based materials in wastewater treatment of petroleum industry, Green Energy Environ., 5 (2020) 37–49.

[5] W.F. Elmobarak, F. Almomani, Application of Fe_3O_4 magnetite nanoparticles grafted in silica (SiO_2) for oil recovery from oil in water emulsions, Chemosphere, 265 (2021) 129054, doi: 10.1016/j.chemosphere.2020.129054.
[6] A. Faraji, M. Cuccarese, S. Masi, I.M. Mancini, D.J. Caniani, Use of carbon materials for produced water treatment: a review on adsorption process and performance, Int. J. Environ. Sci. Technol., (2021) 1–16, doi: 10.1007/s13762-021-03395-y.
[7] R.S. Souza, P.S.S. Porto, A.M.A. Pintor, G. Ruphuy, M.F. Costa, R.A.R. Boaventura, V.J.P. Vilar, New insights on the removal of mineral oil from oil-in-water emulsions using cork by-products: effect of salt and surfactants content, Chem. Eng. J., 285 (2016) 709–717.
[8] H.H. El-Maghrabi, R. Hosny, M. Ramzi, M.A. Zayed, M. Fathy Moubark, Preparation and characterization of novel magnetic $ZnFe_2O_4$–hydroxyapatite core–shell nanocomposite and its use as fixed bed column system for removal of oil residue in oily wastewater samples, Egypt. J. Petrol., 28 (2019) 137–144.
[9] F. Mohammed, A.K. Muhammad Al-Hamidawi, M.H. Azeez Al-buhayder, T.J. Mohammed, Sustainable materials production for oily wastewater treatment, IOP Conf. Ser.: Earth Environ. Sci., 961 (2022) 012080, doi: 10.1088/1755-1315/961/1/012080.
[10] A. Diraki, H.R. Mackey, G. McKay, A. Abdala, Removal of emulsified and dissolved diesel oil from high salinity wastewater by adsorption onto graphene oxide, J. Environ. Chem. Eng., 7 (2019) 103106, doi: 10.1016/j.jece.2019.103106.
[11] J. Ma, X. Fu, W. Xia, R. Zhang, K. Fu, G. Wu, B. Jia, S. Li, J. Li, Removal of emulsified oil from water by using recyclable chitosan based covalently bonded composite magnetic flocculant: performance and mechanism, J. Hazard. Mater., 419 (2021) 126529, doi: 10.1016/j.jhazmat.2021.126529.
[12] K.-Y. Andrew Lin, S.-Y. Chen, Enhanced removal of oil droplets from oil-in-water emulsions using polyethylenimine-modified rice husk, Waste Biomass Valorization, 6 (2015) 495–505.
[13] N.A. Abdelwahab, N. Shukry, S.F. El-kalyoubi, Separation of emulsified oil from wastewater using polystyrene and surfactant modified sugarcane bagasse wastes blend, Clean Technol. Environ. Policy, 23 (2021) 235–249.
[14] S. Nešić, V.V. Streletskaya, An integrated approach for produced water treatment and injection, Georesources, 20 (2018) 25–31.
[15] Y. Liu, H. Lu, Y. Li, H. Xu, Z. Pan, P. Dai, H. Wang, Q. Yang, A review of treatment technologies for produced water in offshore oil and gas fields, Sci. Total Environ., 775 (2021) 145485, doi: 10.1016/j.scitotenv.2021.145485.
[16] U.W.R. Siagian, S. Widodo, Khoiruddin, A.K. Wardani, I. Gede Wenten, Oilfield Produced Water Reuse and Reinjection with Membrane, Membrane Science, Material and Technologies, The 24th Regional Symposium on Chemical Engineering (RSCE 2017), MATEC Web of Conferences, EDP Sciences, 156 (2018) 08005.
[17] S. Jiménez, M.M. Micó, M. Arnaldos, F. Medina, S. Contreras, State of the art of produced water treatment, Chemosphere, 192 (2018) 186–208.
[18] X. Wei, S. Zhang, Y. Han, F.A. Wolfe, Treatment of petrochemical wastewater and produced water from oil and gas, Water Environ. Res., 91 (2019) 1025–1033.
[19] M.A. Al-Ghouti, M.A. Al-Kaabi, M.Y. Ashfaq, D.A. Da'na, Produced water characteristics, treatment and reuse: a review, J. Water Process Eng., 28 (2019) 222–239.
[20] E. Virga, R.W. Field, P. Biesheuvel, W.M. de Vos, Theory of oil fouling for microfiltration and ultrafiltration membranes in produced water treatment, J. Colloid Interface Sci., 621 (2022) 431–439.
[21] F.A. Dawodu, C.J. Abonyi, K.G. Akpomie, Feldspar-banana peel composite adsorbent for efficient crude oil removal from solution, Appl. Water Sci., 11 (2021) 3, doi: 10.1007/s13201-020-01335-8.
[22] E.H. Khader, T.J. Mohammed, N. Mirghaffari, A.D. Salman, T. Juzsakova, T.A. Abdullah, Removal of organic pollutants from produced water by batch adsorption treatment, Clean Technol. Environ. Policy, 24 (2022) 713–720.
[23] B. Zhang, R. Hu, D. Sun, T. Wu, Y. Li, Fabrication of magnetite-graphene oxide/MgAl-layered double hydroxide composites for efficient removal of emulsified oils from various oil-in-water emulsions, J. Chem. Eng. Data, 63 (2018) 4689–4702.
[24] A. Bondarieva, I. Yaichenia, N. Zahorodniuk, V. Tobilko, V. Pavlenko, Water purification from cationic organic dyes using kaolin-based ceramic materials, Ecol. Environ. Technol., 2 (2022) 10–16.
[25] A. Hamd, D. Rady, K.N.M. Elsayed, H. Al Mohamadi, A.M. Elzanaty, S.A. Ahmed, R. El-Sayed, N.K. Soliman, Application of nano bio-clay composite in a scaling-up study for wastewater treatment, Biointerface Res. Appl. Chem., 12 (2022) 6393–6414.
[26] A. Arizavi, N.S. Mirbagheri, Z. Hosseini, P. Chen, S. Sabbaghi, Efficient removal of naphthalene from aqueous solutions using a nanoporous kaolin/Fe_3O_4 composite, Int. J. Environ. Sci. Technol., 17 (2019) 1991–2002.
[27] Z. Huang, J. Bu, H. Wang, Application of two modified kaolin materials in removing micro-plastics from water, J. Mater. Cycles Waste Manage., 24 (2022) 1460–1475.
[28] C. Yu, M. Zhou, X.N. Yu, J.C. Shao, X.Q. Cai, Synthesis of nano-iron supported by graphene oxide/kaolin for the treatment of lead ions contaminated water, Digest J. Nanomater. Biostruct., 14 (2019) 193–202.
[29] A. Gad, B.A. Al-Mur, W.A. Alsiary, S.M. Abd El Bakey, Optimization of carboniferous Egyptian kaolin treatment for pharmaceutical applications, Sustainability, 14 (2022) 2388, doi: 10.3390/su14042388.
[30] I.S. Izman, S.N.A. Baharin, R. Rusmin, Magnetic kaolinite composite for lead removal in aqueous solution, Malaysian J. Anal. Sci., 24 (2020) 115–124.
[31] H. Koyuncu, A.R. Kul, Removal of aniline from aqueous solution by activated kaolinite: kinetic, equilibrium and thermodynamic studies, Colloids Surf., A, 569 (2019) 59–66.
[32] D. Ghosh, K.G. Bhattacharyya, Adsorption of methylene blue on kaolinite, Appl. Clay Sci., 20 (2002) 295–300.
[33] Y. Wang, S. Luo, A. Chen, C. Shang, L. Peng, J. Shao, Z. Liu, Environmentally friendly kaolin-coated meshes with superhydrophilicity and underwater superoleophobicity for oil/water separation, Sep. Purif. Technol., 239 (2020) 116541, doi: 10.1016/j.seppur.2020.116541.
[34] J. Usman, M.H.D. Othman, A.F. Ismail, M.A. Rahman, J. Jaafar, Y.O. Raji, T.H. El Badawy, A.O. Gbadamosi, T.A. Kurniawan, Impact of organosilanes modified superhydrophobic superoleophilic kaolin ceramic membrane on efficiency of oil recovery from produced water, J. Chem. Technol. Biotechnol., 95 (2020) 3300–3315.
[35] R.S. Alkizwini, The use of an organo-kaolinite sorbent in a permeable reactive barrier for remediating groundwater contaminated with methylene blue dye: experimental and theoretical investigation, Environ. Process., 8 (2021) 889–910.
[36] J. Zhu, L. Zhang, S. Zhong, P. Gao, J. Shen, Grainy Nano Zero-Valent Iron With Kaolin Clay and Activated Carbon for Trichloroethylene Degradation: Preparation, Performance, and Mechanism, 2022. Available at SSRN: https://ssrn.com/abstract=4048714 or http://dx.doi.org/10.2139/ssrn.4048714.
[37] K. He, G. Chen, G. Zeng, A. Chen, Z. Huang, J. Shi, M. Peng, T. Huang, L. Hu, Enhanced removal performance for methylene blue by kaolin with graphene oxide modification, J. Taiwan Inst. Chem. Eng., 89 (2018) 77–85.
[38] Y. Zhang, S. Chen, X. Feng, J. Yu, X. Jiang, Self-assembly of sponge-like kaolin/chitosan/reduced graphene oxide composite hydrogels for adsorption of Cr(VI) and AYR, Environ. Sci. Pollut. Res., 26 (2019) 28898–28908.
[39] A. Abdelkhalek, M.A. El-Latif, H. Ibrahim, H. Hamad, M. Showman, Controlled synthesis of graphene oxide/silica hybrid nanocomposites for removal of aromatic pollutants in water, Sci. Rep., 12 (2022) 7060, doi: 10.1038/s41598-022-10602-4.
[40] A. Razaq, F. Bibi, X. Zheng, R. Papadakis, S.H.M. Jafri, H. Li, Review on graphene-, graphene oxide-, reduced graphene oxide-based flexible composites: from fabrication to applications, Materials, 15 (2022) 1012, doi: 10.3390/ma15031012.

[41] S. Elhenawy, M. Khraisheh, F. AlMomani, M.K. Hassan, M.A. Al-Ghouti, R. Selvaraj, Recent developments and advancements in graphene-based technologies for oil spill cleanup and oil-water separation processes, Nanomaterials, 12 (2021) 87, doi: 10.3390/nano12010087.
[42] R.A. Konale, N.K. Mahale, S.T. Ingle, Nano-zeolite-graphene oxide composite for calcium hardness removal: isotherm and kinetic study, Water Pract. Technol., 15 (2020) 1011–1031.
[43] W. Peng, H. Li, Y. Liu, S. Song, A review on heavy metal ions adsorption from water by graphene oxide and its composites, J. Mol. Liq., 230 (2017) 496–504.
[44] S. Thangavel, G. Venugopal, Understanding the adsorption property of graphene-oxide with different degrees of oxidation levels, Powder Technol., 257 (2014) 141–148.
[45] N. Baig, Ihsanullah, M. Sajid, T.A. Saleh, Graphene-based adsorbents for the removal of toxic organic pollutants: a review, J. Environ. Manage., 244 (2019) 370–382.
[46] A. Fakhri, Adsorption characteristics of graphene oxide as a solid adsorbent for aniline removal from aqueous solutions: kinetics, thermodynamics and mechanism studies, J. Saudi Chem. Soc., 21 (2017) S52–S57.
[47] A. Mishra, Study of organic pollutant removal capacity for magnetite@graphene oxide nanocomposites, Vacuum, 157 (2018) 524–529.
[48] S.E. Rokni, R. Haji Seyed Mohammad Shirazi, M. Miralinaghi, E. Moniri, Efficient adsorption of anionic dyes onto magnetic graphene oxide coated with polyethylenimine: kinetic, isotherm, and thermodynamic studies, Res. Chem. Intermed., 46 (2020) 2247–2274.
[49] A. Diraki, H. Mackey, G. McKay, A.A. Abdala, Removal of oil from oil–water emulsions using thermally reduced graphene and graphene nanoplatelets, Chem. Eng. Res. Des., 137 (2018) 47–59.
[50] L.T.M. Thy, N.H. Thuong, T.H. Tu, H.M. Nam, N.H. Hieu, M.T. Phong, Synthesis of magnetic iron oxide/graphene oxide nanocomposites for removal of cadmium ions from water, Adv. Nat. Sci.: Nanosci. Nanotechnol., 10 (2019) 025006, doi: 10.1088/2043-6254/ab1b79.
[51] J. Liu, H. Wang, X. Li, W. Jia, Y. Zhao, S. Ren, Recyclable magnetic graphene oxide for rapid and efficient demulsification of crude oil-in-water emulsion, Fuel, 189 (2017) 79–87.
[52] I.A. Kuranga, A.B. Alafara, F.B. Halimah, A.M. Fausat, O.B. Mercy, B.C. Tripathy, Production and characterization of water treatment coagulant from locally sourced kaolin clays, J. Appl. Sci. Environ. Manage., 22 (2018) 103–109.
[53] S. Abdulsalam, I. Misau, A. Abdulkarim Yusuf, Potentials of alkaleri and kankara kaolinite clay for the production of aluminum sulphate, Int. J. Eng. Res. Appl., 2 (2013) 2008–2012.
[54] S. Mustapha, M.M. Ndamitso, A.S. Abdulkareem, J.O. Tijani, A.K. Mohammed, D.T. Shuaib, Potential of using kaolin as a natural adsorbent for the removal of pollutants from tannery wastewater, Heliyon, 5 (2019) e02923, doi: 10.1016/j.heliyon.2019.e02923.
[55] M. Raji, A.E.K. Qaiss, R. Bouhfid, Effects of bleaching and functionalization of kaolinite on the mechanical and thermal properties of polyamide 6 nanocomposites, RSC Adv, 10 (2020) 4916–4926.
[56] F. Chigondo, B.C. Nyamunda, V. Bhebhe, Extraction of water treatment coagulant from locally abundant kaolin clays, J. Chem., 2015 (2015) 705837, doi: 10.1155/2015/705837.
[57] L.-F. Chen, H.-W. Liang, Y. Lu, C.-H. Cui, S.-H. Yu, Synthesis of an attapulgite clay@carbon nanocomposite adsorbent by a hydrothermal carbonization process and their application in the removal of toxic metal ions from water, Langmuir, 27 (2011) 8998–9004.
[58] X. Qi, Y. Lian, L. Yan, R.L. Smith Jr., One-step preparation of carbonaceous solid acid catalysts by hydrothermal carbonization of glucose for cellulose hydrolysis, Catal. Commun., 57 (2014) 50–54.
[59] F. Quesada-Plata, R. Ruiz-Rosas, E. Morallón, D. Cazorla-Amorós, Activated carbons prepared through H_3PO_4-assisted hydrothermal carbonisation from biomass wastes: porous texture and electrochemical performance, ChemPlusChem, 81 (2016) 1349–1359.
[60] M. Adel, A. El-Maghraby, O. El-Shazly, E.-W.F. El-Wahidy, M.A.A. Mohamed, Synthesis of few-layer graphene-like nanosheets from glucose: new facile approach for graphene-like nanosheets large-scale production, J. Mater. Res., 31 (2016) 455–467.
[61] M. Sevilla, C. Sanchís, T. Valdés-Solís, E. Morallón, A.B. Fuertes, Direct synthesis of graphitic carbon nanostructures from saccharides and their use as electrocatalytic supports, Carbon, 46 (2008) 931–939.
[62] G. Xiao, M. Ni, R. Xiao, X. Gao, K. Cen, Catalytic carbonization of lignin for production of electrically conductive charcoal, J. Biobased Mater. Bioenergy, 6 (2012) 69–74.
[63] M. Fathy, T.A. Moghny, M.A. Mousa, A.-H.A.-A. El-Bellihi, A.E. Awadallah, Synthesis of transparent amorphous carbon thin films from cellulose powder in rice straw, Arabian J. Sci. Eng., 42 (2017) 225–233.
[64] M. Fathy, M.A. Mousa, T.A. Moghny, A.E. Awadallah, Characterization and evaluation of amorphous carbon thin film (ACTF) for sodium ion adsorption, Appl. Water Sci., 7 (2017) 4427–4435.
[65] L.T.M. Thy, P.M. Cuong, T.H. Tu, H.M. Nam, N.H. Hieu, M.T. Phong, Fabrication of magnetic iron oxide/graphene oxide nanocomposites for removal of lead ions from water, Chem. Eng. Trans., 78 (2020) 277–282.
[66] I.M. Sadiana, K. Karelius, R. Agnestisia, A.H. Fatah, Studies on synthesis, characterization, and adsorption of cationic dyes from aqueous solutions using magnetic composite material from natural clay in Central Kalimantan, Indonesia, Molekul, 13 (2018) 63–71, doi: 10.20884/1.jm.2018.13.1.414.
[67] M.R. Lasheen, I.Y. El-Sherif, D.Y. Sabry, S.T. El-Wakeel, M.F. El-Shahat, Adsorption of heavy metals from aqueous solution by magnetite nanoparticles and magnetite-kaolinite nanocomposite: equilibrium, isotherm and kinetic study, Desal. Water Treat., 57 (2015) 17421–17429.
[68] M. Fathy, M. El-Sayed, M. Ramzi, O.H. Abdelraheem, Adsorption separation of condensate oil from produced water using ACTF prepared of oil palm leaves by batch and fixed bed techniques, Egypt. J. Petrol., 27 (2018) 319–326.
[69] J. Wang, A. Shi, D. Agyei, Q. Wang, Formulation of water-in-oil-in-water (W/O/W) emulsions containing *trans*-resveratrol, RSC Adv., 7 (2017) 35917–35927.
[70] S.M. Niknam, I. Escudero, J.M. Benito, Formulation and preparation of water-in-oil-in-water emulsions loaded with a phenolic-rich inner aqueous phase by application of high energy emulsification methods, Foods, 9 (2020) 1411, doi: 10.3390/foods9101411.
[71] K.-Y. Andrew Lin, Y.-C. Chen, S. Phattarapattamawong, Efficient demulsification of oil-in-water emulsions using a zeolitic imidazolate framework: adsorptive removal of oil droplets from water, J. Colloid Interface Sci., 478 (2016) 97–106.
[72] A. Magdy, Y.O. Fouad, M.H. Abdel-Aziz, A.H. Konsowa, Synthesis and characterization of Fe_3O_4/kaolin magnetic nanocomposite and its application in wastewater treatment, J. Ind. Eng. Chem., 56 (2017) 299–311.
[73] H. Wang, Y. Wei, Magnetic graphene oxide modified by chloride imidazole ionic liquid for the high-efficiency adsorption of anionic dyes, RSC Adv., 7 (2017) 9079–9089.
[74] J. Shao, X. Yu, M. Zhou, X. Cai, C. Yu, Nanoscale zero-valent iron decorated on bentonite/graphene oxide for removal of copper ions from aqueous solution, Materials, 11 (2018) 945, doi: 10.3390/ma11060945.
[75] R.V. Xikhongelo, F.M. Mtunzi, P.N. Diagboya, B.I. Olu-Owolabi, R.-A. Düring, Polyamidoamine-functionalized graphene oxide–SBA-15 mesoporous composite: adsorbent for aqueous arsenite, cadmium, ciprofloxacin, ivermectin, and tetracycline, Ind. Eng. Chem. Res., 60 (2021) 3957–3968.
[76] T. Lutfee, J.A. Al-Najar, F.M. Abdulla, Removal of oil from produced water using biosorbent, IOP Conf. Ser.: Mater. Sci. Eng., 737 (2020) 012198, doi: 10.1088/1757-899X/737/1/012198.
[77] S. Long, Y. Feng, Y. Liu, L. Zheng, L. Gan, J. Liu, X. Zeng, M. Long, Renewable and robust biomass carbon aerogel derived from deep eutectic solvents modified cellulose nanofiber under a low carbonization temperature for

oil-water separation, Sep. Purif. Technol., 254 (2021) 117577, doi: 10.1016/j.seppur.2020.117577.
[78] X. Huang, J. Tian, Y. Li, X. Yin, W. Wu, Preparation of a three-dimensional porous graphene oxide–kaolinite–poly(vinyl alcohol) composite for efficient adsorption and removal of ciprofloxacin, Langmuir, 36 (2020) 10895–10904.
[79] T.A. Aragaw, A.N. Alene, A comparative study of acidic, basic, and reactive dyes adsorption from aqueous solution onto kaolin adsorbent: effect of operating parameters, isotherms, kinetics, and thermodynamics, Emerging Contam., 8 (2022) 59–74.